Microstructural characterization of ultrafine-grained nickel

A. P. Zhilyaev[*, 1, 2], **J. Gubicza**[3], **G. Nurislamova**[4], **Á. Révész**[1, 3], **S. Suriñach**[1], **M. D. Baró**[1], and **T. Ungár**[3]

[1] Departament de Física, Grup de Física dels Materials II, Universitat Autònoma de Barcelona, 08193 Bellaterra, Spain
[2] Institute of Mechanics, Russian Academy of Science, 450000 Ufa, Russia
[3] Department of General Physics, Eötvös University, P.O.B. 32, 1518 Budapest, Hungary
[4] Institute for Physics of Advanced Materials, Ufa State Aviation Technical University, 450000 Ufa, Russia

Peak profile analysis based on high-resolution X-ray diffractometry and transmission electron microscopy (TEM) were used to measure the distribution of grain sizes, the dislocation density, and the corresponding root mean square strain in ultrafine-grained (UFG) nickel processed by different methods: electrodeposition, equal channel angular pressing (ECAP), cold rolling (CR), high pressure torsion (HPT), and their combinations. The Fourier transforms of the experimental X-ray peak profiles were fitted by theoretical functions calculated on the basis of the model of the microstructure. In this model the crystallites are assumed to have spherical shape and log-normal size distribution. It is also supposed that the strain broadening of the profiles is caused by $\langle 110 \rangle \{111\}$ type dislocations. The results obtained from X-ray diffraction are compared with TEM micrographs. It is found that additional deformation following ECAP further decreases the crystallite size and increases the dislocation density. However, in the electrodeposited specimen the crystallite size is lower and the dislocation density is higher than in the samples obtained by any of the combinations of the severe plastic deformation (SPD) procedures.

1 Introduction

Ultrafine-grained (UFG) and nanocrystalline (NC) materials are produced with the aim to improve different physical and chemical properties related to their grain size [1]. Properties of UFG and NC materials at the submicron and nanoscale are not necessarily predictable from those observed in their coarse-grained counterparts. Important changes in behavior are caused not only by a continuous modification of the characteristics with refining the microstructure but also by the emergence of entirely new phenomena, e.g. quantum size confinement, wave-like transport, and predominance of interfacial phenomena [2]. It is now well established that electrodeposition [3, 4] and SPD processing [5] can lead to a very significant refinement in the grain size of a wide range of materials including pure metals, metallic alloys, and intermetallics. It was reported that these UFG materials demonstrate unusual physical properties such as a decrease in the elastic moduli, a decrease in the Curie and Debye temperatures, an increase in the rates of diffusion, and improved magnetic properties [6–8]. If the UFG metals and alloys are reasonably stable at elevated temperatures, there is a potential for achieving superplastic ductility at relatively low testing temperatures and high strain rates [8, 9]. Very recent results have shown that SPD processed materials

* Corresponding author: e-mail: Alex.Zhilyaev@uab.es

may combine high strength and high ductility [10] where this atypical combination can be attributed to the development of UFG and nanostructures.

Pure Ni represents a useful model material for the investigation of processing by severe plastic deformation [11]. On the one hand, the lower stacking fault energy (SFE) in comparison with pure aluminum leads to more extensive refinement in the as-processed materials. On the other hand, since Ni has a higher SFE than Cu, the microstructure in Ni becomes more homogeneous.

Several authors have made TEM investigations on the microstructure of Ni samples processed by SPD including ECAP [11, 12], HPT [13], and by electrodeposition [9, 14–16]. In recent reports it was noted that the microstructure after ECAP shows arrays of reasonably equiaxed grains but the grain boundaries are irregularly arranged and poorly defined, suggesting a high-energy non-equilibrium configuration with large internal stresses. HPT straining [13] can produce UFG microstructure that may not be fully homogeneous across the sample cross-section. It was concluded that in order to obtain samples with the desired homogeneous UFG microstructure, they have to be processed at applied pressure values higher than 6 GPa and with more than five whole revolutions. It was reported that electrodeposition can lead to more extensive refinement of Ni with a nanocrystalline microstructure of 20–40 nm.

The highly strained microstructure of SPD materials can only be characterized locally by transmission electron microscopy. In this sense high-resolution X-ray diffraction has the advantage of providing information on the mean grain size and a function of grain size distribution, internal microstrains, and related dislocation densities [17, 18]. It is especially useful in the case of UFG metals and alloys produced by SPD where the measurement of the very high dislocation densities (10^{15}–10^{16} m^{-2}) is complicated by TEM. The complete characterization of the microstructure can be achieved by simultaneous application of X-ray diffraction and TEM. This paper reports new results of the measurement of crystallite size and size distribution and the dislocation density in SPD processed pure nickel by means of high-resolution X-ray diffraction. The deformation was carried out by ECAP, HPT, cold rolling (CD), and their combinations. An additional specimen was produced by electrodeposition. The results of the X-ray diffraction peak profile analysis are compared with TEM analysis and discussed in terms of correlations and discrepancies.

2 Materials and experimental

High-purity nickel (99.99%) was deformed by different methods of SPD, i.e., equal channel angular pressing (ECAP), cold rolling (CR), high-pressure torsion (HPT), and their combinations. The principles of severe plastic deformation by ECAP and HPT have been documented in several papers [5, 6, 11–13]. Nickel cylinders having diameters of 16 mm and lengths of ≈100 mm were subjected to ECAP at room temperature using a die with an internal angle of 90°. Samples were pressed repetitively for eight passes, equivalent to a total strain of ≈8, and each sample was reversed from end to end and rotated by 90° about the longitudinal axis between passes. Earlier experiments showed that this procedure produces an as-pressed mean grain size of ≈0.35 μm [12]. For processing by HPT, disks with diameters of 10 mm and thicknesses of ≈0.3 mm were torsionally strained under a high pressure of 6 GPa for a total of five complete revolutions, equivalent to a true logarithmic strain of ≈6. This procedure produces a mean grain size of ≈0.17 μm [13]. Three additional samples were prepared by a combination of different methods: (i) ECAP and cold rolling (denoted as ECAP + CR), (ii) ECAP and HPT (denoted as ECAP + HPT), and (iii) the combination of three deformation modes (denoted as ECAP + CR + HPT). Cold rolling of ECAP specimens was performed at room temperature with a total reduction in the thickness from 1.7 to 0.25 mm, equivalent to a reduction of ≈85%. Figure 1 shows schematically all processing routes. In addition, a sample of electrodeposited nanocrystalline nickel with a grain size of ≈35 nm was also included for comparison with the deformed specimens. The microstructure of the samples was examined using high-resolution X-ray diffraction.

The diffraction profiles were measured by a special high-resolution double-crystal diffractometer with negligible instrument-induced broadening [19, 20]. The Nonius FR591 rotating copper anode ($\lambda = 0.15406$ nm) was operated at 40 kV and 70 mA. The K$_{\alpha2}$ peak of the Cu radiation was eliminated by
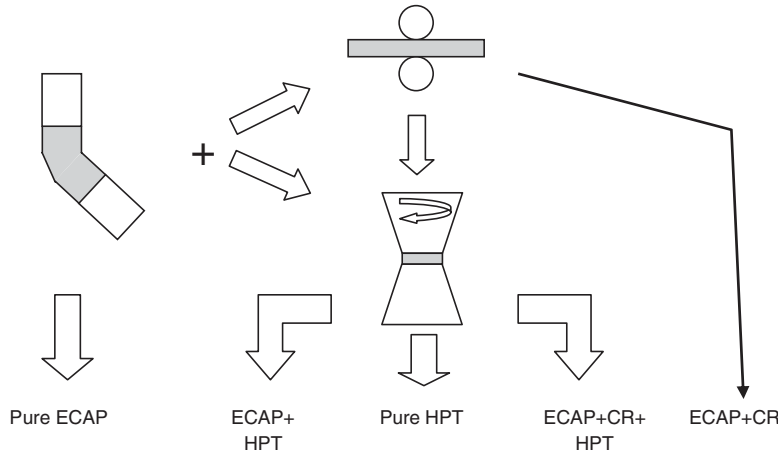
Fig. 1 Schematic representation of ultrafine-grained nickel processing.

a 0.16 mm slit placed between the source and the symmetrically cut 220 Ge monochromator. The profiles were recorded by a linear position sensitive gas-flow detector (OED 50 Braun, Munich). Selected samples were examined by transmission electron microscopy (TEM) using a JEM-100B electron microscope.

3 Evaluation of the X-ray diffraction profiles

A numerical procedure has been worked out for fitting the Fourier transform of the experimental profiles by the product of the theoretical functions of the size and the distortion (strain) Fourier transforms (multiple whole profile fitting, MWP) [17, 18]. The theoretical functions were calculated from a microstructural model with the following assumptions: (i) the crystallites are spheres and have log-normal crystallite size distribution and (ii) the lattice distortions are caused by dislocations. From the median, m, and the variance, σ, of the size distribution the arithmetically, the area-, and the volume-weighted mean crystallite size values can be obtained [17]. Since the area-weighted mean grain size was determined from TEM micrographs, the same weighted mean crystallite size is calculated from the results of X-ray diffraction profile analysis. The area-weighted mean crystallite size was determined from m and σ using the equation [17]

$$\langle d \rangle_{\text{area}} = m \exp\left(2.5\sigma^2\right). \tag{1}$$

The distortion (or strain) Fourier coefficients of a peak profile, A^{D}, in a dislocated crystal can be given as [21]

$$A^{\mathrm{D}}(L) = \exp\left[-\rho B L^2 f(\eta)\, g^2 \bar{C}\right], \tag{2}$$

where $B = \pi b^2/2$, b is the absolute value of the Burgers vector of the dislocation, ρ is the dislocation density, L is the column length normal to the diffracting plane defined as $L = na_3$, where $a_3 = \lambda/2(\sin\theta_2 - \sin\theta_1)$, n are integers starting from zero, $\eta = L/R_{\mathrm{e}}$, R_{e} is the effective outer cut-off radius of the dislocations, g is the absolute value of the diffraction vector, $\bar{C}$ is the average dislocation contrast factor, and $f(\eta)$ is a function derived explicitly by Wilkens (see Eqs. A.6 to A.8 in Ref. [22] and Eqs. (22) and (23) in Ref. [17]). Instead of R_{e}, it is more appropriate to use the parameter $M = R_{\mathrm{e}}\rho^{1/2}$ defined by Wilkens as the dislocation arrangement parameter [22]. In an untextured cubic polycrystalline specimen the values of $\bar{C}$ can be expressed as a function of the indices of reflections, hkl [23],

$$\bar{C} = \bar{C}_{h00}[1 - q(h^2 k^2 + h^2 l^2 + k^2 l^2)/(h^2 + k^2 + l^2)^2], \tag{3}$$

where $\overline{C}_{h00}$ is the average dislocation contrast factor for the $h00$ reflections and q is a parameter depending on the elastic constants of the crystal and on the character of dislocations (e.g., edge or screw type).

The MWP method has the following steps:

the Fourier coefficients of the measured physical profiles are calculated by a non-equidistant sampling Fourier transformation,

the Fourier coefficients of the size and strain profiles are calculated, and

the experimental and the calculated Fourier coefficients are compared by the least squares method.

The procedure has five fitting parameters for cubic crystals: the median, m, and the variance, σ, of the log-normal size distribution function, the dislocation density, ρ, the dislocation arrangement parameter, M, and q for the average dislocation contrast factors. The values of q have been calculated for nickel assuming the most common dislocation slip system $\langle 110 \rangle \{111\}$. For pure screw or pure edge dislocations the numerically calculated values of q are 2.24 or 1.42, respectively [24]. Consequently, the value of q gives the edge or screw character of dislocations. The dimensionless parameter $M = R_e \rho^{1/2}$ defined as the dislocation arrangement parameter gives the strength of the dipole character of dislocations: the higher the value of M, the weaker the dipole character and the screening of the displacement fields of dislocations. Further details of the fitting procedure are given elsewhere [17, 18].

4   Results and discussion

The procedure of X-ray peak profile fitting was carried out for all specimens studied here. Figure 2 represents an example of the fitting for nickel produced by ECAP. The figure shows the experimentally determined Fourier transforms (open circles) and the best fitted theoretical curves (solid lines). The differences between the measured and fitted values are also shown in the lower part of the figure. The scaling of the differences is the same as in the main part of the figure. The indices of the reflections are also indicated. As the result of the fitting, the microstructural parameters are determined and listed in Table 1.

Figure 3 shows the crystallite size distribution for three different processing methods, ECAP, HPT, and electrodeposition. One can see from Fig. 3 and Table 1 that HPT results in higher dislocation densities and lower mean crystallite size values during deformation than ECAP. At the same time, the HPT process leads to narrower distributions of crystallite size compared to ECAP. The method of electrodeposition gives smaller crystallite size and a higher dislocation density than any of the SPD methods. On the other hand, the electrodeposited nickel has the widest crystallite size distribution among all the materials studied here.
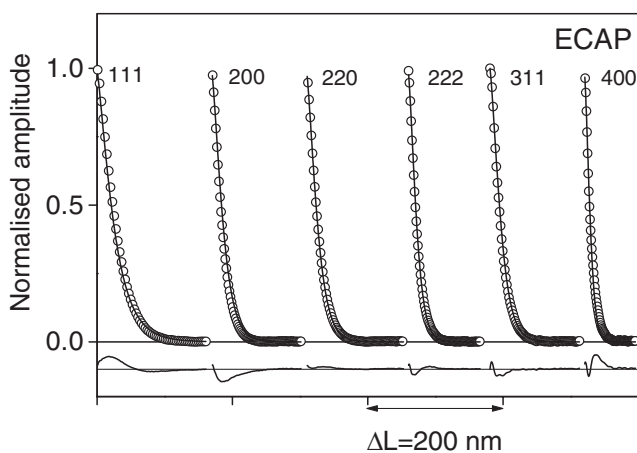

Fig. 2 Measured (open circles) and fitted (solid line) Fourier coefficients as a function of L for the ECAP nickel sample. The differences between the measured and fitted values are also shown at the bottom of the figure at the same scale.
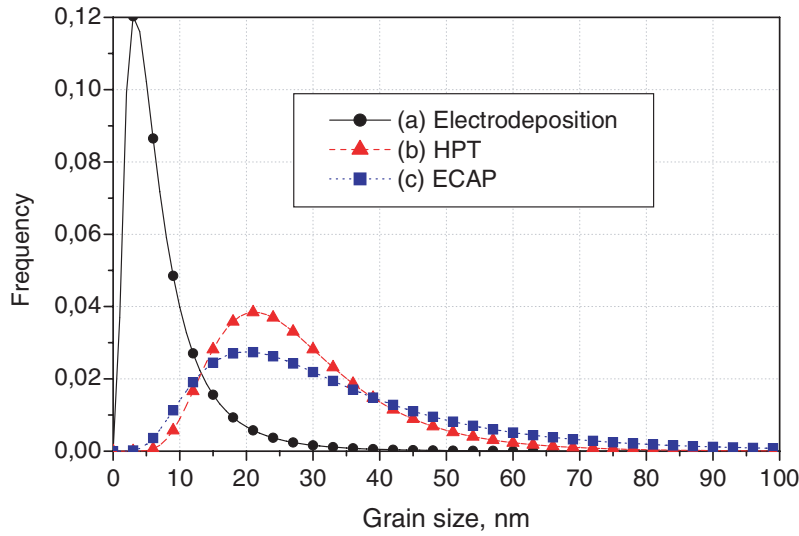
Fig. 3 (online colour at: www.interscience.wiley.com) Crystallite size distributions for nickel samples obtained by three different methods: electrodeposition (a), high-pressure torsion (b), and equal channel angular pressing (c).

The method of high-resolution X-ray diffraction allows to make some conclusions about the type of dislocations prevailing in the present samples. The ECAP nickel has a mixed type of dislocation since $q = 1.84$, which is equal to the average q values for pure screw ($q = 2.24$) and edge ($q = 1.42$) dislocations. On the contrary, the HPT samples show a tendency to have dislocations of more screw character ($q = 2.16$). This can be interpreted in terms of the rotational mode of deformation. The character of dislocations in the electrodeposited material is more of the edge type ($q = 1.66$).

Figure 4 represents the grain size distributions for the nickel samples which were subjected to a subsequent deformation process after ECAP to increase the total strain: ECAP, ECAP + CR, ECAP + HPT, and ECAP + CR + HPT. It can be seen from Fig. 4 and Table 1 that any of the second steps of subsequent deformation after ECAP results in a reduction in the crystallite size. Applying three deformation methods after each other (ECAP + CR + HPT), a further crystallite size refinement is achieved, and the size distribution is broadened compared to the two-step deformed samples. It can be established that the density and the dipole character of the dislocation structure increases by applying additional deformation after ECAP. The increase in the dislocation density is higher for ECAP + HPT than for ECAP + CR. The combination of ECAP + CR + HPT does not result in a higher dislocation density compared to ECAP + HPT. At the same time, the incorporation of cold-rolling between ECAP and HPT gives a

Table 1 Microstructural parameters for nickel samples processed by different methods.

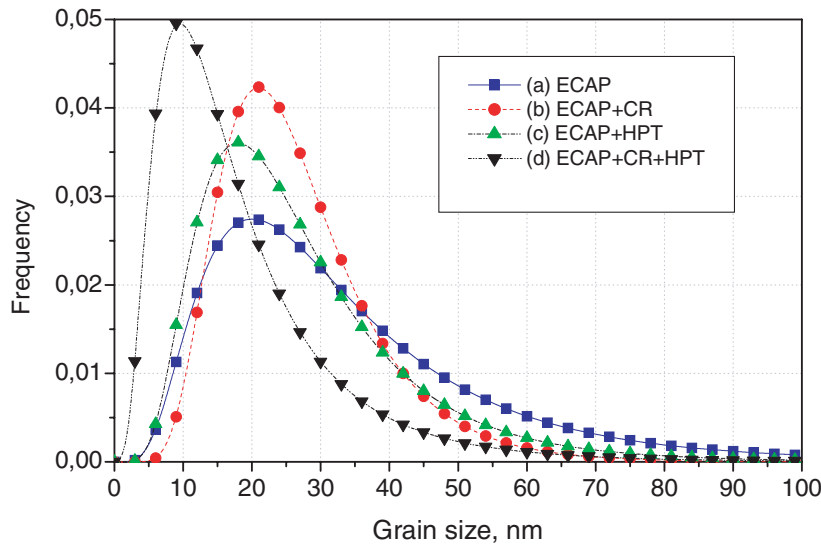| Nickel samples	m	σ	$\langle d \rangle_{area}$	d_{TEM}	$\langle \varepsilon^2 \rangle^{1/2}$	q	M	$\rho, 10^{14}$ m^{-2}	
	nm		nm	nm	10^{-3}			X-ray	DSC [25]
ECAP	29 ± 2	0.60 ± 0.05	71 ± 5	350	2.5 ± 0.3	1.84 ± 0.06	3.7 ± 0.4	9 ± 1	0.4
ECAP + CR	25 ± 2	0.41 ± 0.05	38 ± 4	300	2.6 ± 0.3	2.18 ± 0.06	1.5 ± 0.3	11 ± 1	0.6
HPT	26 ± 2	0.44 ± 0.04	42 ± 4	170	3.1 ± 0.3	2.16 ± 0.05	1.5 ± 0.4	17 ± 2	0.7
ECAP + HPT	24 ± 2	0.53 ± 0.05	48 ± 4	140	3.7 ± 0.4	1.64 ± 0.06	1.5 ± 0.2	25 ± 2	1.9
ECAP + CR + HPT	15 ± 1	0.67 ± 0.06	46 ± 3	100	3.5 ± 0.4	1.61 ± 0.05	2.3 ± 0.3	20 ± 2	2.1
electro-dep.	6 ± 1	0.76 ± 0.06	24 ± 3	35	7.0 ± 0.5	1.66 ± 0.07	4.1 ± 0.4	82 ± 4	6

Fig. 4 (online colour at: www.interscience.wiley.com)   Crystallite size distributions for nickel samples obtained by combinations of different methods: ECAP (a), ECAP + cold rolling (b), ECAP + high-pressure torsion (c), and ECAP + cold rolling + high-pressure torsion (d).

broader crystallite size distribution with a lower mean size (see Table 1). It has been found that the smallest crystallite size and the highest dislocation density is obtained by electrodeposition. No definite conclusion can be made on the edge or screw character of dislocation ensembles formed during two- or three-step processing.

The dislocation density of ECAP and HPT samples of nickel is of the same order of magnitude as reported by other authors [5]. The values of the dislocation density for all nickel samples are about one order of magnitude higher than the dislocation density evaluated for the same material in [25] from differential scanning calorimetry (DSC) experiments. The difference can be attributed to the simple model employed in the evaluation of stored elastic energy, which does not take into account the character of dislocations and their arrangement.

The root mean square strain due to the dislocation structure was determined for the 400 reflection at the value of $L = 0.5$ nm using the Eq. [22]

$$\left\langle \varepsilon_{g,L}^2 \right\rangle \approx \left(\frac{\rho \bar{C} b^2}{4\pi} \right) \ln \left(\frac{R_e}{L} \right). \tag{4}$$

In this calculation, the values of ρ and R_e obtained from the MWP fitting procedure were used. The root mean square strain values are listed in Table 1 and they correlate well with the values of the dislocation density.

Figures 5a–f show TEM micrographs for UFG nickel specimens produced by ECAP, ECAP + CR, HPT, ECAP + HPT, ECAP + CR + HPT, and electrodeposition, respectively. The assumption made for the shape of the crystallites in the evaluation of the X-ray profiles is supported by the TEM micrographs of Fig. 5 since the crystallites seem to be fairly equiaxed. The examination of the TEM pictures in Fig. 5 reveals several common features associated with these samples. All of the SPD processes lead to highly non-equilibrium microstructures with many grain boundaries that are poorly defined and with grain interiors having complex contrast. These observations suggest a high level of internal stresses and elastic distortions of the crystal lattice. Former TEM studies showed that the materials processed by SPD techniques may also possess distinctive inhomogeneities [11, 13]. Thus, HPT samples generally exhibit some variation in the microstructure between the center and the edge of the disk [13], whereas samples processed by ECAP have an anisotropy of grain-shape along the pressing direction [12]. In the present inves
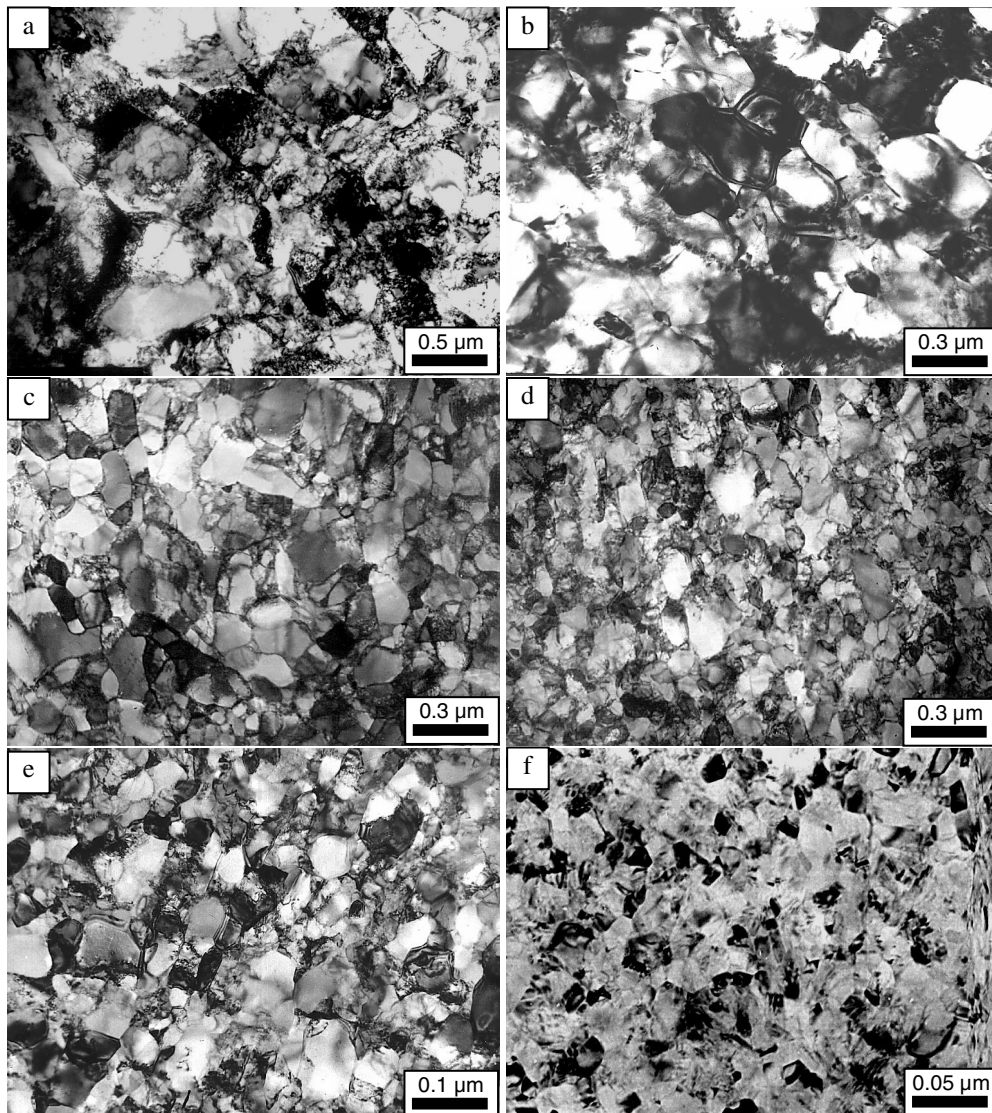
Fig. 5 Microstructure of UFG nickel processed by a) ECAP, b) ECAP + CR, c) HPT, d) ECAP + HPT, e) ECAP + CR + HPT, and f) electrodeposited nickel.

tigation, the use of a combination of ECAP and HPT provides an opportunity for removing some of these undesirable properties and for strong refinement of the microstructure. Figure 5d shows a TEM micrograph of nickel after ECAP + HPT processing, while Fig. 5e demonstrates the microstructure obtained by combination of ECAP, cold rolling, and HPT. Under these conditions, the microstructure is rather homogeneous with the mean grain size of ≈140 nm for ECAP + HPT and about 100 nm for ECAP + CR + HPT. In agreement with the X-ray analysis, the refinement of the microstructure during the subsequent SPD process after ECAP can be seen by comparing Figs. 5a, d, and e. The difference in the crystallite and grain size values determined by X-ray and TEM, respectively, cannot be attributed to the assumption concerning the log-normal crystallite size distribution, since this affects only slightly the results obtained for the average crystallite size values [17].

It is informative to compare the grain and the crystallite size values obtained by TEM and X-ray diffraction. For the ECAP-processed nickel the mean crystallite size obtained by X-ray (71 nm) is about five times smaller than the value of 350 nm evaluated by TEM. A similar tendency is observed for the nickel sample produced by HPT, but the difference is smaller between the crystallite size obtained by X-ray diffraction (42 nm) and the grain size determined by TEM (170 nm). The nickel samples produced by the combination of SPD methods have a mean grain size of 48 and 46 nm for ECAP + HPT and ECAP + CR + HPT, respectively. The evaluation of TEM micrographs for the same samples gives about 140 and 100 nm, respectively. As it has been shown by the X-ray analysis, the three-step deformation (ECAP + CR + HPT) resulted in a broader size distribution of the crystallites with a lower median than ECAP + HPT, which can also be observed by comparing Figs. 5d and e. For the electrodeposited nickel, both X-ray and TEM evaluations give the smallest crystallite (24 nm) or grain size (35 nm) values among the materials studied. It is worth to note that for the electrodeposited nickel sample the area-weighted mean crystallite size value is comparable with the mean grain size obtained from TEM.

The difference between the crystallite sizes obtained by X-ray and the grain size values determined by microscopy techniques describes the complexity of the microstructure. For the ECAP deformed nickel sample, the TEM study gives a mean grain size value of about 350 nm [12] and orientation imaging microscopy [26] with a sensitivity angle $\theta < 2°$ leads to a value of about 270 nm, while the X-ray analysis results in an area-weighted crystallite size of 71 nm.

Each characteristic size value describes a certain feature of the microstructure in ECAP nickel: $\langle d \rangle_{TEM} \approx 350$ nm corresponds to the average distance between high-angle grain boundaries, $\langle d \rangle_{OIM} \approx 270$ nm gives the typical distance between all grain boundaries with misorientations higher than 2°, and $\langle d \rangle_{X-ray} \approx 71$ nm relates to the average size of the coherently scattering domains which usually equals the dislocation cell size in SPD materials. The neighboring dislocation cells separated by small-angle grain boundaries have a misorientation of less than 2°, which cannot be detected by conventional TEM. At the same time, X-ray diffraction makes a difference between the neighboring dislocation cells bordered by small-angle grain boundaries, which usually results in a smaller grain size than that determined by TEM. This preposition is supported also by comparison of the ECAP and ECAP + CR samples. Although the grain sizes obtained by TEM (350 and 300 nm) are very close to each other, a notable difference can be found in the crystallite sizes determined by X-ray diffraction (71 and 38 nm). This is the consequence of the formation of dense tangles of dislocations arranged in low-angle boundaries during cold rolling.

4 Concluding remarks

High-resolution X-ray diffraction and TEM experiments were conducted to determine the microstructure and dislocation density in ultrafine-grained materials after processing by ECAP, HPT, cold rolling, and their combinations. Additionally to the nanostructured materials produced by SPD, electrodeposited nickel has been investigated, too. Assuming that the crystallite size distribution in all samples obeys a log-normal function and that the strains are caused by dislocations, the parameters of the crystallite size distribution and the dislocation structure were calculated by fitting the Fourier transforms of the experimental X-ray diffraction profiles to physically well established theoretical functions. The crystallite size values were compared to the grain sizes determined by TEM. It was found that the additional deformation after ECAP resulted in a further grain refinement and an increase of the dislocation density. However, electrodeposition has given even finer microstructure and higher dislocation density than the materials processed by SPD methods. The crystallite size values are lower than the grain size for all the specimens, since the former measures the dislocation cell size in SPD materials. At the same time, for the electrodeposited nickel the crystallite size is close to the grain size determined by TEM.

References

[1] H. Gleiter, Acta Mater. **48**, 1 (2000).
[2] Y. T. Zhu, T. G. Langdon, R. S. Mishra, S. L. Semiatin, M. J. Saran, and T. C. Lowe (eds.), Ultrafine Grained Materials II (TMS, Warrendale (PA), 2002).
[3] S. Kaja, H. W. Pickering, and W. R. Bitler, Plat. Surf. Finish. **73**, 58 (1986).
[4] E. Toth-Kadar, I. Bakonyi, L. Pogany, and A. Cziraki, Surf. Coat. Technol. **88**, 57 (1996).
[5] R. Z. Valiev, R. K. Islamgaliev, and I. V. Alexandrov, Prog. Mater. Sci. **45**, 103 (2000).
[6] R. Z. Valiev, A. V. Korznikov, and R. R. Mulyukov, Mater. Sci. Eng. A **168**, 141 (1993).
[7] Yu. R. Kolobov and R. Z. Valiev (eds.), Grain Boundary Diffusion and Properties of Nanostructured Materials (Nauka, Novosibirsk, 2001) (in Russian).
[8] S. X. McFadden, R. S. Mishra, R. Z. Valiev, A. P. Zhilyaev, and A. K. Mukherjee, Nature **398**, 684 (1999).
[9] S. X. McFadden, A. P. Zhilyaev, R. S. Mishra, and A. K. Mukherjee, Mater. Lett. **45**, 345 (2000).
[10] R. Z. Valiev, I. V. Alexandrov, Y. T. Zhu, and T. C. Lowe, J. Mater. Res. **17**, 5 (2002).
[11] K. Neishi, Z. Horita, and T. G. Langdon, Mater. Sci. Eng. A **325**, 54 (2002).
[12] A. P. Zhilyaev, G. V. Nurislamova, M. D. Baró, R. Z. Valiev, and T. G. Langdon, Metall. Mater. Trans. A **33**, 1865 (2002).
[13] A. P. Zhilyaev, S. Lee, G. V. Nurislamova, R. Z. Valiev, and T. G. Langdon, Scr. Metall. Mater. **44**, 2753 (2001).
[14] J. A. Eastman, M. R. Fitzsimmons, and L. J. Thompson, Philos. Mag. B **66**, 667 (1992).
[15] A. Cziraki, Zs. Tonkovics, I. Gerocs, B. Fogarassy, I. Groma, E. Toth-Kadar, T. Tarnoczi, and I. Bakonyi, Mater. Sci. Eng. A **179/180**, 531 (1994).
[16] N. Wang, Z. Wang, K. T. Aust, and U. Erb, Acta Mater. **45**, 1655 (1997).
[17] T. Ungár, J. Gubicza, G. Ribárik, and A. Borbély, J. Appl. Crystallogr. **34**, 298 (2001).
[18] G. Ribárik, T. Ungár, and J. Gubicza, J. Appl. Crystallogr. **34**, 669 (2001).
[19] M. Wilkens and H. Eckert. Z. Naturforsch. A **19**, 459 (1964).
[20] T. Ungár, L. S. Tóth, J. Illy, and I. Kovács, Acta Metall. **34**, 1257 (1986).
[21] W. C. Hinds, Aerosol Technology: Properties, Behavior and Measurement of Airbone Particles Wiley, (New York 1982).
[22] M. Wilkens, in: Fundamental Aspects of Dislocation Theory, Vol. II, edited by J. A. Simmons, R. de Wit, and R. Bullough, Nat. Bur. Stand. (US) Spec. Publ. **317**, (Washington, DC, 1970), p. 1195.
[23] T. Ungár and G. Tichy, phys. stat. sol. (a) **171**, 425 (1999).
[24] T. Ungár, I. Dragomir, Á. Révész, and A. Borbély J. Appl. Crystallogr. **32**, 992 (1999).
[25] A. P. Zhilyaev, G. V. Nurislamova, S. Suriñach, M. D. Barò, and T. G. Langdon, Mater. Phys. Mech. **5**, 23 (2002).
[26] A. P. Zhilyaev, B.-K. Kim, G. V. Nurislamova, M. D. Baró, J. A. Szpunar, and T. G. Langdon, Scr. Metall. Mater. **46**, 575 (2002).